Monthly Weather Review

A Filtering Method for Gravitationally Stratified Flows

Caroline Gatti-Bono

cbono@llnl.gov

Phillip Colella (Corresponding author)

pcolella@lbl.gov

Computational Research Division

Lawrence Berkeley National Laboratory

One Cyclotron Road Mail Stop 50A-1148

Berkeley, CA 94720-8142

Submitted on 04/25/2005

Abstract

Gravity waves arise in gravitationally stratified compressible flows at low Mach and Froude numbers. These waves can have a negligible influence on the overall dynamics of the fluid but, for numerical methods where the acoustic waves are treated implicitly, they impose a significant restriction on the time step. A way to alleviate this restriction is to filter out the modes corresponding to the fastest gravity waves so that a larger time step can be used. This paper presents a filtering strategy of the fully compressible equations based on normal mode analysis that is used throughout the simulation to compute the fast dynamics and that is able to damp only fast gravity modes.

Key words:

Non-hydrostatic atmospheric model; embedded-boundary method; all-speed; gravity waves; normal mode analysis; filtering

Introduction

Gravity waves are present in gravitationally stratified compressible flows at low Mach and Froude numbers, such as atmospheric and stellar flows. For mesoscale simulations, these waves can have a negligible influence on the overall dynamics of the fluid (Jablonowski [4]). However, computationally, they impose a sharp restriction on the time step for methods where the advection is treated explicitly and the acoustic dynamics implicitly. Therefore, methods have been designed to filter out these waves so that a larger time step can be used. One strategy is to remove the fast gravity waves from the initial data by using a normal mode analysis, as shown by Temperton and Williamson ([5] and [9]), Temperton [6] and Tribbia ([7] and [8]). Another strategy is to use divergence damping (Jablonowski [4]) to filter out the high-frequency variations of the velocity divergence field throughout the simulation. This method, however, does not selectively damp the different gravity waves, and might remove some waves that are actually important for the dynamics of the system. In this paper, we propose a filtering strategy of the fully compressible equations based on normal mode analysis that is used throughout the simulation to compute the fast dynamics and that damps only specific gravity modes.

The method is based on the asymptotic analysis presented in Gatti-Bono and Colella ([3]) and it can be used with a wide variety of numerical methods for compressible equations since it only requires that the acoustic dynamics be treated implicitly. The components associated with the fast dynamics are computed using vertical normal eigenmodes and corresponding one-dimensional horizontal wave equations obtained from an asymptotic analysis ([3]). The method is tested on a series of idealized examples, including the mountain lee-waves problem from Durran [1].

1 Isolating Normal Modes

In this section, we summarize our strategy to identify the normal modes of an atmospheric flow. A detailed version can be found in [3].

We start by considering an inviscid compressible fluid described by the compressible Euler equations in perturbational form

$$\frac{\partial \tilde{\rho}}{\partial t} + div(\tilde{\rho}\mathbf{u}) + div(\rho_o \mathbf{u}) = 0 \tag{1}$$

$$\frac{\partial \mathbf{u}}{\partial t} + \mathbf{u} \cdot \mathbf{grad}(\mathbf{u}) + \frac{1}{\rho}\mathbf{grad}\tilde{p} + \frac{\tilde{\rho}}{\rho} g\mathbf{k} = 0 \tag{2}$$

$$\frac{\partial \tilde{p}}{\partial t} + \mathbf{u} \cdot \mathbf{grad}(\tilde{p}) + \rho c^2 div(\mathbf{u}) - w\rho_o g = 0 \tag{3}$$

Here, $\rho_o(z)$ is the hydrostatic density, $\tilde{\rho} = \rho - \rho_o$ is the perturbational density,

$p_o(z)$ is the hydrostatic pressure defined as

$$\frac{dp_o}{dz} = -\rho_o g \tag{4}$$

and $\tilde{p} = p - p_o$ is the perturbational pressure.

These equations contain different time scales: those of acoustic waves, gravity-waves and advection, that are intertwined in the current form of the Euler equations. To separate out the different time scales so that we can later obtain the normal modes of the system, we introduce a splitting of the velocity and the pressure that can be obtained through projections

$$\mathbf{u} = \mathbf{u}_d + \mathbf{u}_p + \mathbf{u}_h \tag{5}$$

$$p = p_o + \pi_H + \pi_I + \psi + \delta \tag{6}$$

where $\mathbf{u}$ is the total velocity, $\mathbf{u}_d$ is the anelastic velocity, $\mathbf{u}_p$ is the curl-free velocity, $\mathbf{u}_h$ is the harmonic velocity, π_H is the "hydrostatic-like" pressure associated with the gravity waves, π_I is the pressure associated with the incompressible effects, ψ is the pressure that corresponds to the vertical motions generated by the horizontal gravity waves and δ is the acoustic pressure.

The velocities are defined as

$$\mathbf{u}_d = \mathbb{P}_o(\mathbf{u}) \tag{7}$$

$$\mathbf{u}_p = \mathbb{Q}_o(\mathbf{u}) \tag{8}$$

where

$$\mathbb{Q}_o(\mathbf{w}) = \mathbf{grad}\left(\mathbb{L}_{\frac{1}{\eta_o}}\right)^{-1} div\,(\eta_o \mathbf{w}) \tag{9}$$

$$\mathbb{P}_o(\mathbf{w}) = (\mathbb{I} - \mathbb{Q}_o)\,(\mathbf{w}) \tag{10}$$

and satisfy

$$div\,(\eta_o \mathbf{u}_d) = 0 \tag{11}$$

$$\mathbf{u}_p = \mathbf{grad}(\varphi) \tag{12}$$

$$\mathbf{u}_h = \mathbf{grad}(\upsilon)\,; \quad div\,(\eta_o \mathbf{grad}(\upsilon)) = 0 \tag{13}$$

The function η_o is chosen to be

$$\frac{1}{\eta_o}\frac{d\eta_o}{dz} = -\frac{\rho_o g}{\gamma p_o} = \frac{1}{\gamma p_o}\frac{dp_o}{dz} \qquad \eta_o(0) = \rho_o(0) \tag{14}$$

and the details can be found in [3]. We note that η_o corresponds to the isentropic density associated with the pressure distribution p_o, and also that equation (11) is a constraint similar to the pseudo-incompressible constraint introduced by Durran [2]. However, the constraint is imposed only on the anelastic part of the velocity here, whereas it was imposed on the total velocity in [2]. The pressures satisfy

$$\frac{\partial \pi_H}{\partial z} = -\tilde{\rho} g \tag{15}$$

$$\frac{1}{\rho}\Big(\mathbf{grad}\pi_I\Big) = -\mathbb{Q}_\rho\left(\mathbf{A_d u}\right) \tag{16}$$

$$\frac{1}{\rho}\mathbf{grad}(\psi) = -\mathbb{Q}_\rho\left(\frac{1}{\rho}\frac{\partial \pi_H}{\partial x}\mathbf{i}\right) \tag{17}$$

$$\delta = p - p_o(z) - \pi - \psi \tag{18}$$

with

$$\mathbb{Q}_\rho \mathbf{w} = \frac{1}{\rho}\mathbf{grad}\left(\mathbb{L}_{\frac{\rho}{\eta_o}}\right)^{-1} div\left(\eta_o \mathbf{w}\right) \tag{19}$$

$$\mathbf{A_d u} = \left(\mathbf{u}\cdot\mathbf{grad}\right)\mathbf{u} - \mathbf{grad}\left(\frac{|\mathbf{u_p}+\mathbf{u_h}|^2}{2}\right) \tag{20}$$

Using the splitting, equations (1)–(4) become

$$\frac{\partial \tilde{\rho}}{\partial t} - \frac{\rho_o N^2}{g} w + div(\tilde{\rho}\mathbf{u}) + \frac{\rho_o}{\eta_o} div(\eta_o \mathbf{u}_p) = 0 \tag{21}$$

$$\begin{aligned}\frac{\partial \mathbf{u}_d}{\partial t} + \mathbf{A}_d\mathbf{u} + \frac{1}{\rho}\mathbf{grad}(\pi_I) + \frac{1}{\rho}\frac{\partial \pi_H}{\partial x}\mathbf{i} + \frac{1}{\rho}\mathbf{grad}(\psi) \\ +\mathbb{P}_o\left[\frac{1}{\rho}\mathbf{grad}\delta + \mathbf{grad}\frac{|\mathbf{u}_p+\mathbf{u}_h|^2}{2}\right] = 0\end{aligned} \tag{22}$$

$$\frac{\partial \mathbf{u}_p}{\partial t} + \mathbb{Q}_o\left[\frac{1}{\rho}\mathbf{grad}\delta + \mathbf{grad}\frac{|\mathbf{u}_p+\mathbf{u}_h|^2}{2}\right] = 0 \tag{23}$$

$$\begin{aligned}\frac{\partial \delta}{\partial t} + \frac{\partial \pi_H}{\partial t} + \frac{\partial \pi_I}{\partial t} + \frac{\partial \psi}{\partial t} + \mathbf{u}\cdot\mathbf{grad}(\pi_I + \pi_H + \delta + \psi) \\ +\frac{\rho c^2}{\eta_o} div(\eta_o \mathbf{u}_p) + (\pi_I + \pi_H + \delta + \psi)\frac{\rho_o g w}{p_o} = 0\end{aligned} \tag{24}$$

where N is the Brunt-Väisälä frequency defined by

$$\frac{N^2}{g} = \frac{1}{\eta_o}\frac{d\eta_o}{dz} - \frac{1}{\rho_o}\frac{d\rho_o}{dz} \tag{25}$$

Equations (21)–(22) can be cast into a system of hyperbolic equations

$$\begin{aligned}
\mathcal{L}_z \frac{\partial \pi_H}{\partial t} + \eta_o \frac{\partial u_d}{\partial x} &= -\frac{\partial}{\partial z}\left\{ \frac{\eta_o g}{\rho_o N^2}\left[div(\tilde{\rho} u) + \frac{1}{c_0^2}\frac{\partial \pi_H}{\partial t}\right] + \frac{g}{N^2} div(\eta_0 \mathbf{u}_p)\right\} \\
&\quad + div(\eta_o \mathbf{u}_p) + \frac{\eta_o}{\rho_o c_o^2}\frac{\partial \pi_H}{\partial t} - \frac{\partial \eta_o u_p}{\partial x} \qquad (26) \\
\frac{\partial u_d}{\partial t} + \frac{1}{\rho_o}\frac{\partial \pi_H}{\partial x} &= -\left((\mathbf{A}_d \mathbf{u})_x + \frac{1}{\rho}\frac{\partial \pi_I}{\partial x} + \left(\frac{1}{\rho} - \frac{1}{\rho_o}\right)\frac{\partial \pi_H}{\partial x} + \frac{\partial u_p}{\partial t} \right. \\
&\quad \left. + \left[\frac{1}{\rho}\frac{\partial \delta}{\partial x} + \frac{\partial}{\partial x}\left(\frac{|\mathbf{u}_p + \mathbf{u}_h|^2}{2}\right)\right]\right) \qquad (27)
\end{aligned}$$

where

$$\mathcal{L}_z = -\frac{\partial}{\partial z}\left[\frac{\eta_o g}{\rho_o N^2}\left(\frac{1}{g}\frac{\partial}{\partial z} + \frac{1}{c_o^2}\right)\right] + \frac{\eta_o}{\rho_o c_o^2} = -\xi\left[\frac{\partial}{\partial z}\zeta\frac{\partial}{\partial z} + \chi\right] \qquad (28)$$

and

$$\begin{aligned}
\xi &= exp\left(-\int_o^z \frac{g}{c_o^2} dz\right) \qquad (29) \\
\zeta &= \frac{\eta_o}{\rho_o N^2} exp\left(\int_o^z \frac{g}{c_o^2} dz\right) \qquad (30) \\
\chi &= \frac{\eta_o}{\rho_o c_o^2}\left[(\gamma - 1)\frac{g^2}{N^2 c_o^2} - 1\right] exp\left(\int_o^z \frac{g}{c_o^2} dz\right) \qquad (31)
\end{aligned}$$

Asymptotic analysis along with a change of variables ([3]) shows that

$$\begin{aligned}
\hat{\mathcal{L}}_z \frac{\partial \hat{\pi}_H}{\partial t} + \frac{\partial \hat{u}_d}{\partial x} &= O(\varepsilon^2) \qquad (32) \\
\frac{\partial \hat{u}_d}{\partial t} + \frac{\partial \hat{\pi}_H}{\partial x} &= O(\varepsilon^2) \qquad (33)
\end{aligned}$$

where

$$\hat{\pi}_H = \sqrt{\frac{\eta_o}{\rho_o \xi}}\pi_H \qquad (34)$$

$$\hat{u}_d = \sqrt{\frac{\rho_o \eta_o}{\xi}} u_d \tag{35}$$

$$\hat{\mathcal{L}}_z = \sqrt{\frac{\rho_o}{\eta_o \xi}} \mathcal{L}_z \sqrt{\frac{\rho_o \xi}{\eta_o}} \tag{36}$$

and where ε is the aspect ratio, *i.e.* the ratio of the vertical and horizontal length scales.

When χ is negative, the operator $\hat{\mathcal{L}}_z$ is positive definite and equations (26)–(27) describe the motion of an infinite collection of horizontally propagating gravity waves, one for each eigenmode of the second-order self-adjoint operator $\mathcal{L}_z$. $\hat{\mathcal{L}}_z$ has eigenvectors r_k and eigenvalues λ_k, and the eigenvalues λ_k are related to the gravity wave speeds c_k by

$$c_k = \frac{1}{\sqrt{\lambda_k}} \tag{37}$$

Figure 1 shows the gravity wave speeds for the first example presented in the results section along with the four first eigenmodes. As expected, only a few modes travel with a speed larger than a typical mean fluid velocity of $20\, m/s$ (solid line) and the number of sign changes in the eigenmode increases as the mode number increases.

When χ is positive, the first few eigenvalues can become negative, and this is a direct consequence of including the potential dynamics into the asymptotic analysis. We observe that this has a stabilizing effect as the

modes with negative eigenvalues do not support gravity waves.

2 Filtering Normal Modes

This section presents a filtering algorithm that can be applied to any numerical method that solves for the fully compressible equations, as long as the acoustic waves are treated implicitly. The filtering below relies on two related variables that can be extracted from any scheme: the perturbational density defined as $\tilde{\rho} = \rho - \rho_o$ and the pressure term π_H defined as $\dfrac{\partial \pi_H}{\partial z} = -\tilde{\rho} g$. We also need initial data for the one-dimensional anelastic velocity $\hat{u}_d^k$ and pressure term π_H^k for each of the K fastest modes chosen for filtering.

- First, we solve for $\pi_H^{k,n+1}$

$$\left(I - \frac{\Delta t^2}{\lambda^k}\frac{\partial^2}{\partial x^2}\right)\left(\hat{\pi}_H^{k,n+1}\right)^{Fast} = \left(\hat{\pi}_H^{k,n}\right)^{Fast} - \frac{\Delta t}{\lambda^k}\frac{\partial \hat{u}_d^{k,n}}{\partial x} \qquad k \in \{0, 1, \ldots, K\} \tag{38}$$

  where

$$\frac{\partial \hat{u}_d^{k,n}}{\partial x} = -\lambda^k \frac{\left(\hat{\pi}_H^{k,n}\right)^{Fast} - \left(\hat{\pi}_H^{k,n-1}\right)^{Fast}}{\Delta t} \tag{39}$$

- We use equation (21) to advance the perturbational density $\tilde{\rho}$

$$\tilde{\rho}^{n+1} = \tilde{\rho}^n + \Delta t \left(\frac{\partial \tilde{\rho}}{\partial t}\right)^{n+\frac{1}{2}} \tag{40}$$

- Equation (15) is used to advance π_H

$$\pi_H^{n+1} = \int_z^L \tilde{\rho}^{n+1} g d\check{z} \qquad \left(\pi_H(L) = 0\right) \tag{41}$$

- We filter out fast modes in π_H and $\tilde{\rho}$ as soon as we obtain the updated values and before using them in the computation of other variables

$$\left(\pi_H^{n+1}\right)^f = \pi_H^{n+1} - \mathcal{P}_{Fast}\left(\pi_H^{n+1}\right) + \left(\pi_H^{n+1}\right)^{Fast} \tag{42}$$

$$\left(\tilde{\rho}^{n+1}\right)^f = -\frac{1}{g}\frac{\partial\left(\pi_H^{n+1}\right)^f}{\partial z} \tag{43}$$

$$\left(\rho^{n+1}\right)^f = \left(\tilde{\rho}^{n+1}\right)^f + \rho_o \tag{44}$$

where

$$\left(\pi_H^{n+1}\right)^{Fast} = \sqrt{\frac{\rho_o \xi}{\eta_o}} \sum_0^K \left(\hat{\pi}_H^{k,\,n+1}\right)^{Fast} r^k \tag{45}$$

$$\mathcal{P}_{Fast}\left(\pi_H^{n+1}\right) = \sqrt{\frac{\rho_o \xi}{\eta_o}} \sum_0^K \left(\int_0^L \sqrt{\frac{\eta_o}{\rho_o \xi}} \pi_H^{n+1} r^k dz\right) r^k \tag{46}$$

In the following section, we will use this filtering technique in the particular context of the algorithm presented in [3].

3 Results

3.1 Perturbational Gravity-Wave Test Problem

In [3], we set up an example to verify numerically that the algorithm and the splitting of the fully compressible equations allow us to recover results from the asymptotic analysis. We initialize the different variables so that, initially, we have a Gaussian distribution in selected modes only. In [3], we showed that, if the initial data is only in the fastest mode, the wave propagated in that mode only when we used a time step that was smaller than the one dictated by the CFL condition associated with the fastest gravity wave. Here, we add the filtering algorithm as discussed above for the fastest gravity mode ($K = 1$), and we show that the computation is stable for time steps that are larger than the one dictated by the CFL condition associated with the fastest gravity wave. We also use examples in which the initial data is not in the fastest (filtered) mode.

3.1.1 Summary of the Initialization

The solenoidal velocity is initialized as

$$\hat{u}_d(x, z, t = 0) = \sum_{k \in \{k_1, k_2, \ldots, k_p\}} G_k(x) r^k(x) \tag{47}$$

where $k_1, k_2, \ldots, k_p$ is a selection of mode numbers, r^k is the eigenvector in the k^{th} mode and $G_k(x)$ is a Gaussian function

$$G_k(x) = \frac{\alpha_k}{\sqrt{2\pi\sigma}} exp\left(-\frac{(x-x_o)^2}{2\sigma^2}\right) \tag{48}$$

and the pressure π_H is

$$\pi_H(x, z, t=0) = \rho_o \sum_{k\in\{k_1,k_2,\ldots\}} c^k G_k(x) r^k(x) \tag{49}$$

where c^k is the speed of the k^{th} gravity-wave.

The remaining variables are initialized according to their definitions or the equations of motion [3].

3.1.2 Example 1: Initial Data in the Fastest Mode Only

In this example, the initial data is chosen so that it is only in the fastest mode: $k_1 = 0$ and $p = 1$. We use different domain sizes which correspond to different aspect ratios of the computational domain ε and different grid refinements, as shown in Table 1.

Figure 2 shows the projection onto the fast mode of the horizontal velocity and of the pressure π_H for different time steps with filtering and without filtering. The fastest (respectively second fastest) gravity wave propagates with a speed of $164\,m/s$ (respectively $54.7\,m/s$), and to match the CFL

conditions for an aspect ratio of $\varepsilon = 0.0125$ and a grid of 128×64, we have to use a time step smaller than $48.7\,s$ (respectively $146\,s$). Figure 2 shows that the filtering preserves the shape and propagation speed, but introduces some damping in the solution, which is expected because a Helmholtz solve is used to compute the one-dimensional fast solution. However, it should be noted that the filtering of just this one mode alone allows us to multiply the time step by a factor of 3 without losing important features of the solution, whereas the unfiltered solution becomes unstable after just a couple of time steps. Also note that this is an artificial example that focuses on the fastest mode of the solution when, for most mesoscale atmospheric modeling, the few fastest gravity waves are not significant for the dynamics but restrict the time step significantly (Jablonowski [4]). Therefore, ultimately, we do not expect that some damping in the fastest mode would generate accuracy issues for mesoscale simulations.

Figure 3 shows that the solution is in the asymptotic regime for an aspect ratio of $\varepsilon = 0.0125$, and that for this aspect ratio, the damping diminishes when the grid is refined. Note that the curves for $\mathcal{P}_f(\pi_H)$ when the time and grid size are held constant but the aspect ratio changes are superimposed. This is because the initial data is in the first mode and we are filtering that

same mode using (42).

3.1.3 Example 2: Initial Data in Modes 2 and 3

Here, we use two different sets of initial data. For case (a), the initial data is only in the second mode (*i.e.* $k_1 = 2$ and $p = 1$) and for case (b), it is a combination of data in the second and third modes (*i.e.* $k_1 = 2$, $k_2 = 3$ and $p = 2$). Figure 4 shows the projections of the divergence-free velocity and pressure π_H onto the second mode for case (a) (top) and for case (b) (middle) and onto the third mode for case (b) (bottom). These graphs show that the filtering method only has a negligible effect on the accuracy of the solution at fixed time step when the filtered mode is not present in the initial data. Unlike results in the previous section, filtering does not introduce damping. When the time step is multiplied by three, very little damping is introduced and the solution is almost identical to the one for a smaller time step that satisfies the CFL condition for the fastest gravity wave.

3.2 Mountain Lee-Waves

This is the classical example of two-dimensional mountain lee-waves that can be found in Durran [1]. A detailed description of the initial conditions and

parameters can be found in Gatti-Bono and Colella [3]. In this example, a uniform wind flows from left to right at a speed of $20\,m/s$ over a $600\,m$ high mountain. The mountain has the classic witch of Agnesi profile

$$z_{Mountain}(x) = \frac{ha}{(x - x_o)^2 + a^2} \tag{50}$$

with a width a of $10\,km$, a height h of $600\,m$ and a center x_o positioned at $72\,km$. The atmosphere is a two-layered atmosphere with a constant Brunt-Väisälä frequency N of $0.01\,s^{-1}$ or $0.02\,s^{-1}$.

Figure 5 shows the mountain lee-waves example run with and without filtering at different time steps for the unstable cases, *i.e.* the cases where gravity waves are expected. The filtering of the fastest gravity mode ($K = 1$) allows us to double the time step but damps the gravity wave response since this response is essentially in the first mode. However, the main features of the solution are retained when filtering is used. It is interesting to note that this example shows that the filtering method can be used successfully when an embedded-boundary is present and in a two-layered atmospheric setting with a significant gravity-wave response present.

Conclusion

This paper presents a method to filter gravity waves out of the fully compressible equations that is based on normal mode analysis. It can be used in any scheme that treats acoustic waves implicitly. A series of examples were presented to test the filtering method on the algorithm presented in [3]. The method was shown to damp only the modes that are being filtered, keeping the main features of the solution, like wavelengths, unaltered. It was also run successfully on the mountain lee-wave example with embedded-boundaries. In both sets of examples, the computation with filtering was stable when the time step was multiplied by a factor of two or three whereas the computation without filtering would grow unstable after only a few time steps.

Acknowledgement

We would like to acknowledge Dr. Joseph Tribbia for suggesting that we look at the vertical normal mode analysis.

References

[1] Durran D., 1986: Another Look At Downslope Windstorms. Part I: The Development of Analogs to Supercritical Flow in an Infinitely Deep, Continuously Stratified Fluid, *J. Atmos. Sci.*, **43**(21), pp.2527–2543.

[2] Durran D., 1989: Improving the Anelastic Approximation, *J. Atmos. Sci.*, **46**(11), pp.1453–1461.

[3] Gatti-Bono C. and Colella P.: An Anelastic Allspeed Projection Method for Gravitationally Stratified Flows, *J. Comp. Phys.* (submitted).

[4] Jablonowski C., 2004: Adaptive Grids in Weather and Climate Modeling. PhD. dissertation, University of Michigan, 292 pp.

[5] Temperton C., Williamson D.L., 1981: Normal Mode Initialization for a Multilevel Grid-Point Model. Part I: Linear Aspects, *Mon. Wea. Rev.*, **109**, pp.729–743.

[6] Temperton C., 1977: Implicit Normal Mode Initialization, *Mon. Wea. Rev.*, **116**, pp.1013–1031.

[7] Baer F. and Tribbia J.J., 1977: On Complete Filtering of Gravity Modes through Nonlinear Initialization, *Mon. Wea. Rev.*, **105**, pp.1536–1539.

[8] Tribbia J.J., 1984: A Simple Scheme for High-Order Nonlinear Normal Mode Initialization, *Mon. Wea. Rev.*, **112**, pp.278–284.

[9] Williamson D.L., Temperton C., 1981: Normal Mode Initialization for a Multilevel Grid-Point Model. Part I: Nonlinear Aspects, *Mon. Wea. Rev.*, **109**, pp.744–7757.

	$\varepsilon = 0.05$	$\varepsilon = 0.025$	$\varepsilon = 0.0125$	$\varepsilon = 0.00625$
Domain length (km)	256	512	1024	2048
Domain height (km)	12.8	12.8	12.8	12.8

Table 1: Different cases used for the asymptotic analysis.

Figure 1: Gravity wave speeds (left) and vertical eigenmodes (right) for mode number 0 (blue), 1 (green), 2 (red), and 3 (pink).

Figure 2: $\mathcal{P}_f(u_d)$ (left) and $\mathcal{P}_f(\pi_H)$ (right), above for a fixed aspect ratio of 0.0125 and a fixed grid size of 128×64: $40\,s$ (green), $40\,s$ without filtering (red), $80\,s$ (pink), and $120\,s$ (blue).

Figure 3: $\mathcal{P}_f(u_d)$ (left) and $\mathcal{P}_f(\pi_H)$ (right), above for a time step of $120\,s$ for different aspect ratios holding the grid size fixed at 128×64: 0.05 (red), 0.025 (green), 0.0125 (blue), 0.00625 (pink); and below for different resolutions holding the aspect ratio fixed at 0.0125: 64×32 (blue), 128×64 (green), 256×128 (pink). Note that on the graph for $\mathcal{P}_f(\pi_H)$ on top, the three curves are superimposed and appear as if there were only one curve plotted.

Figure 4: $\mathcal{P}_{f_2}(u_d)$ (left) and $\mathcal{P}_{f_2}(\pi_H)$ (right) for an aspect ratio of 0.0125 holding the grid size fixed at 128×64 for $\Delta t = 40\,s$ without filtering (red), $\Delta t = 40\,s$ with filtering (green), $\Delta t = 120\,s$ with filtering (pink); above for an initial data in Mode 2 only (case (a)), middle for an initial data in modes 2 and 3 (case (b)) and bottom, $\mathcal{P}_{f_3}(u_d)$ (left) and $\mathcal{P}_{f_3}(\pi_H)$ (right) for an

initial data in modes 2 and 3 (case (b)). $\mathcal{P}_{f_2}$ ($\mathcal{P}_{f_3}$) is the projection onto the second (third) fastest mode.

Figure 5 Isentropes for a two-layered atmosphere flowing over a $600\,m$ high mountain at $t = 10000\,s$ for an interface at a quarter wavelength (a) $\Delta t = 30\,s$ with filtering and (b) $\Delta t = 15\,s$ with no filtering, and for an interface at a half wavelength (c) $\Delta t = 30\,s$ with filtering and (d) $\Delta t = 15\,s$ with no filtering.

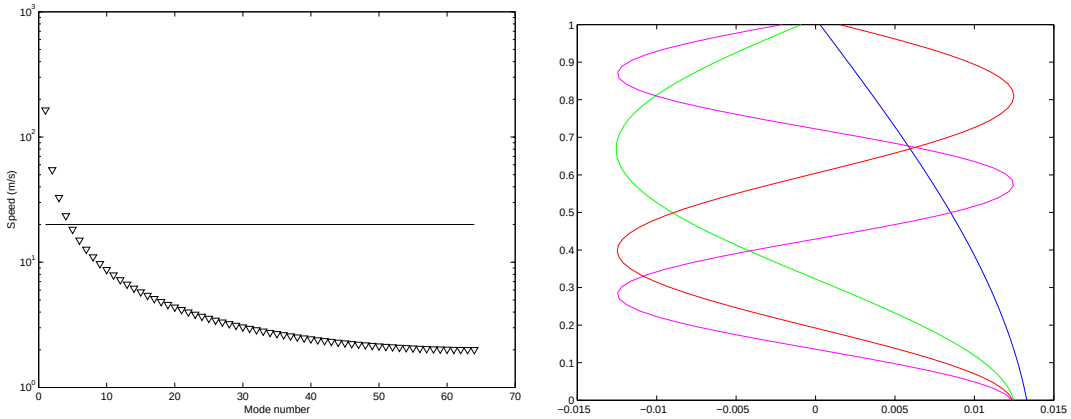

Figure 1: Gravity wave speeds (left) and vertical eigenmodes (right) for mode number 0 (blue), 1 (green), 2 (red), and 3 (pink).

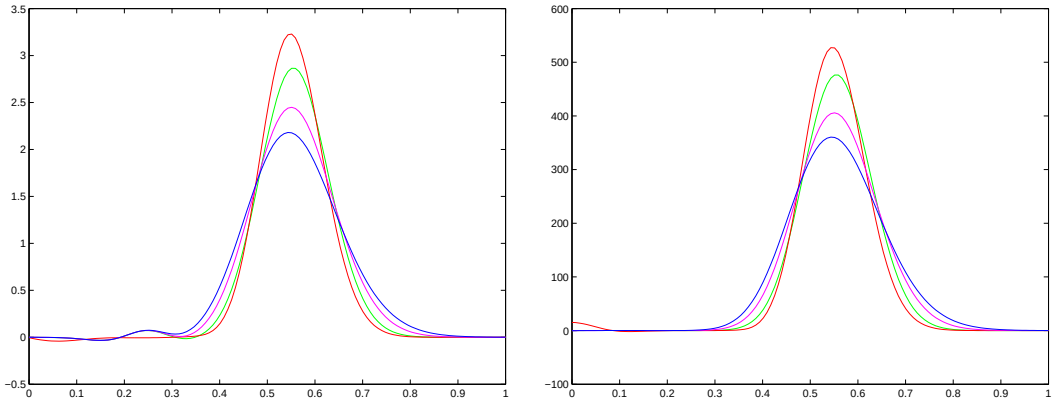

Figure 2: $\mathcal{P}_f(u_d)$ (left) and $\mathcal{P}_f(\pi_H)$ (right), above for a fixed aspect ratio of 0.0125 and a fixed grid size of 128×64: $40\,s$ (green), $40\,s$ without filtering (red), $80\,s$ (pink), and $120\,s$ (blue).

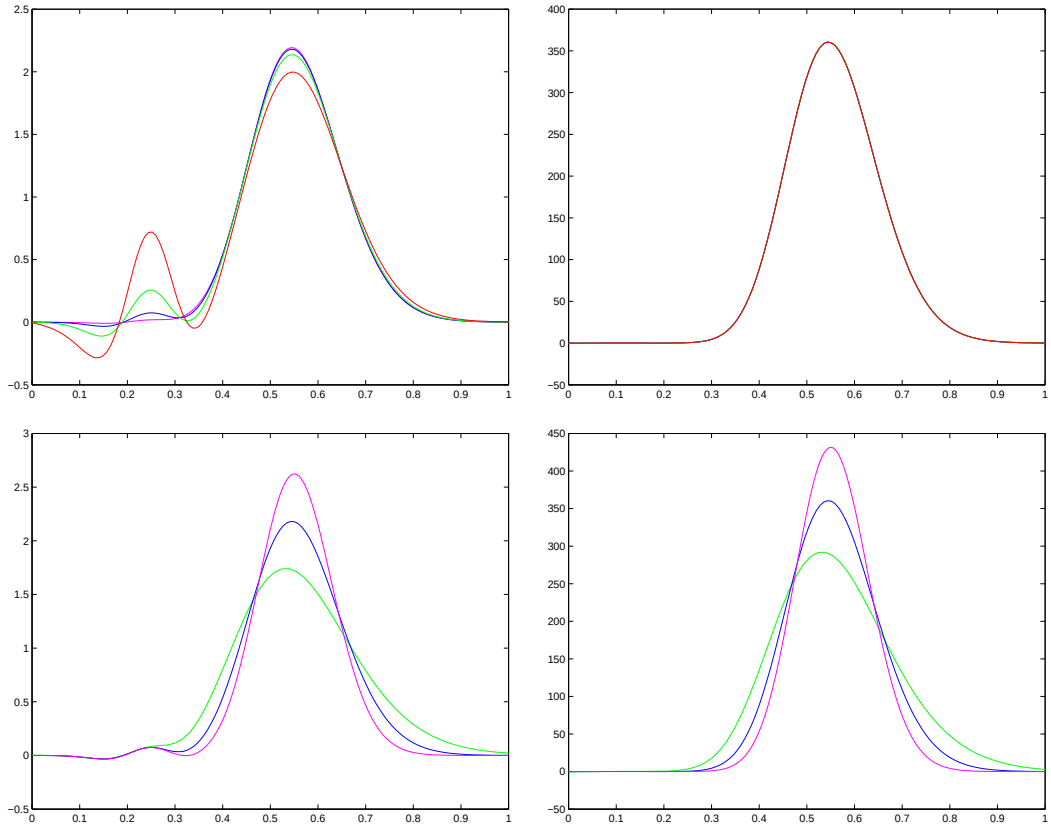

Figure 3: $\mathcal{P}_f\left(u_d\right)$ (left) and $\mathcal{P}_f\left(\pi_H\right)$ (right), above for a time step of $120\,s$ for different aspect ratios holding the grid size fixed at 128×64: 0.05 (red), 0.025 (green), 0.0125 (blue), 0.00625 (pink); and below for different resolutions holding the aspect ratio fixed at 0.0125: 64×32 (blue), 128×64 (green), 256×128 (pink). Note that on the graph for $\mathcal{P}_f(\pi_H)$ on top, the three curves are superimposed and appear as if there were only one curve plotted.

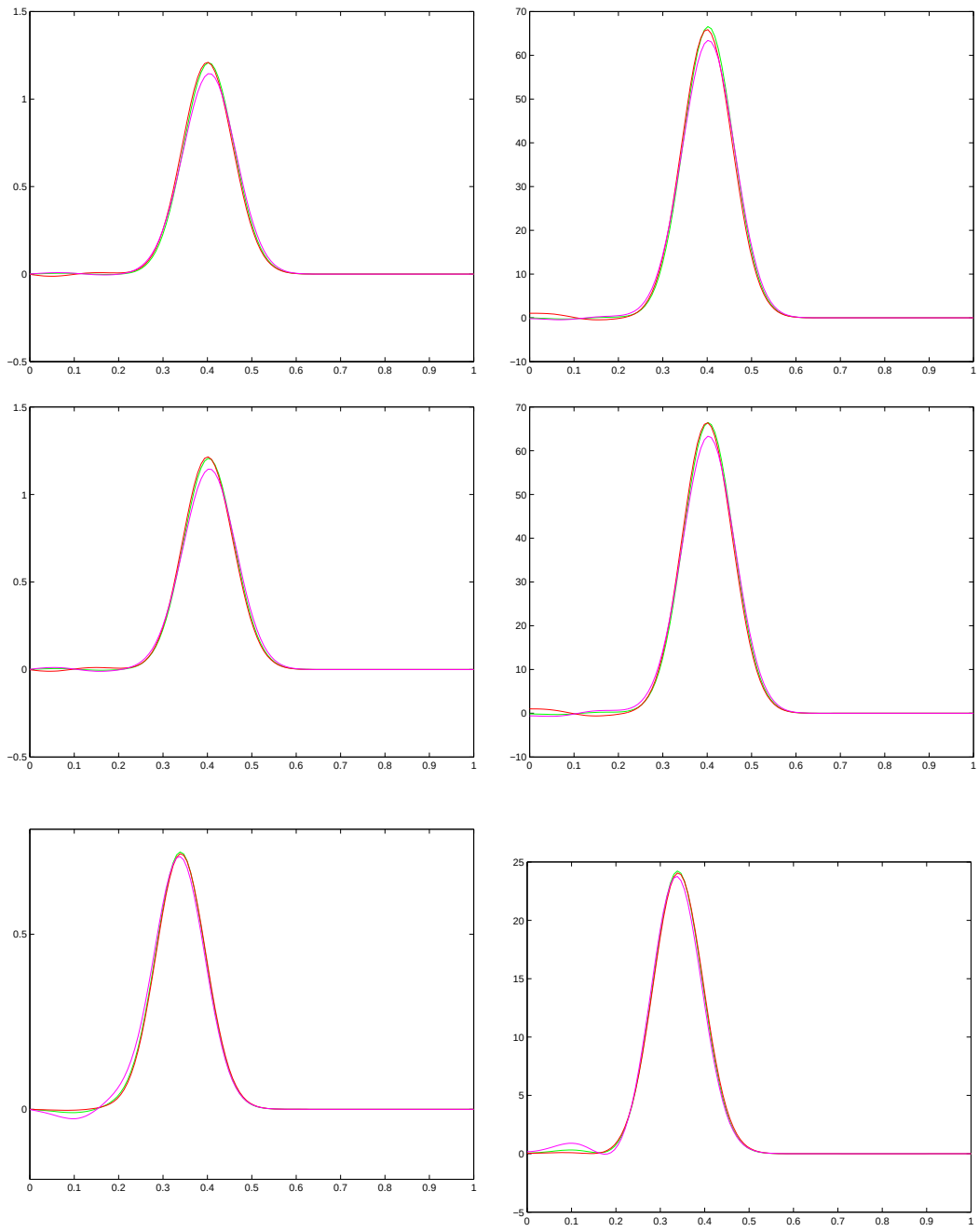

Figure 4: $\mathcal{P}_{f_2}(u_d)$ (left) and $\mathcal{P}_{f_2}(\pi_H)$ (right) for an aspect ratio of 0.0125 holding the grid size fixed at 128×64 for $\Delta t = 40\,s$ without filtering (red), $\Delta t = 40\,s$ with filtering (green), $\Delta t = 120\,s$ with filtering (pink); above for an initial data in Mode 2 only (case (a)), middle for an initial data in modes 2 and 3 (case (b)) and bottom, $\mathcal{P}_{f_3}(u_d)$ (left) and $\mathcal{P}_{f_3}(\pi_H)$ (right) for an initial data in modes 2 and 3 (case (b)). $\mathcal{P}_{f_2}$ ($\mathcal{P}_{f_3}$) is the projection onto the second (third) fastest mode.

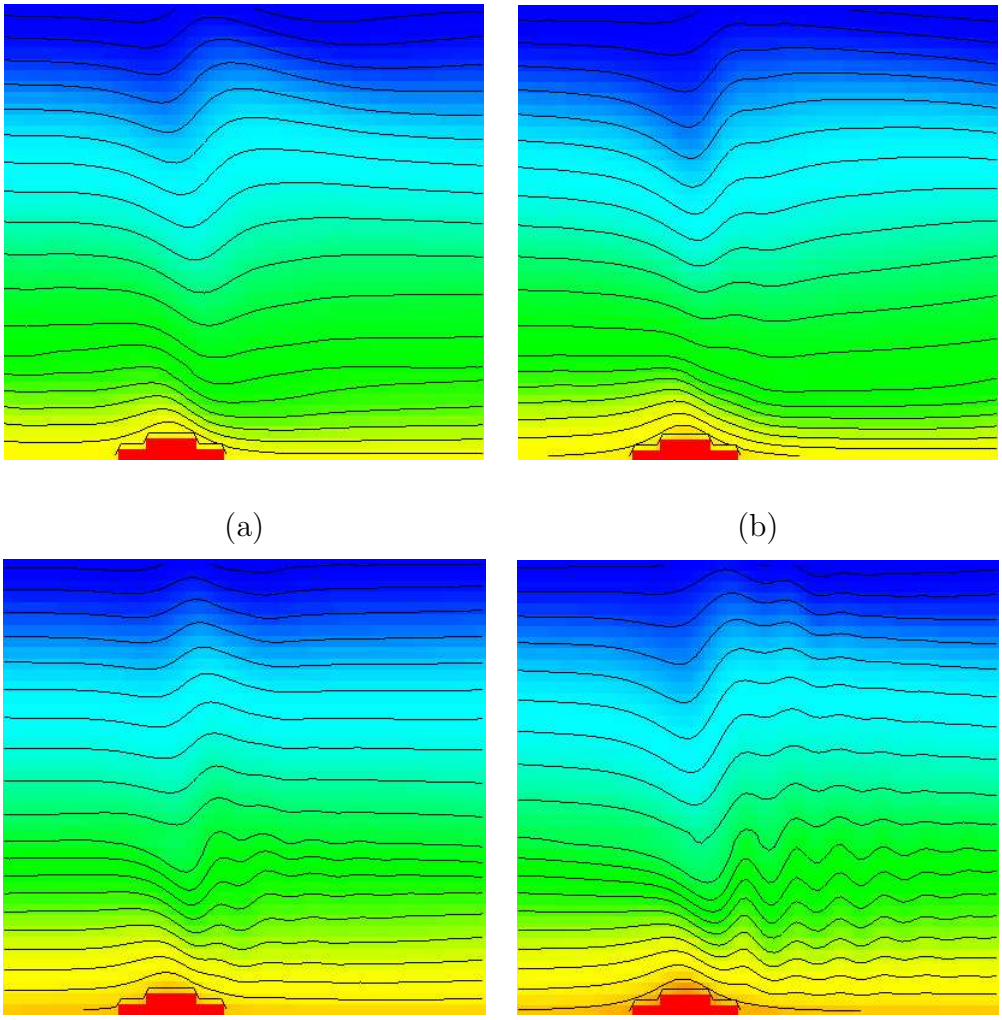

(a) (b)

(c) (d)

Figure 5: Isentropes for a two-layered atmosphere flowing over a 600 m high mountain at $t = 10000\,s$ for an interface at a quarter wavelength (a) $\Delta t = 30\,s$ with filtering and (b) $\Delta t = 15\,s$ with no filtering, and for an interface at a half wavelength (c) $\Delta t = 30\,s$ with filtering and (d) $\Delta t = 15\,s$ with no filtering.